Enhanced Coupling of Superconductivity and Evolution of the Gap Structure in CsV_3Sb_5 via Ta Doping

Yiwen Li(李易文)[1], Zhengyan Zhu(朱政彦)[1], Qing Li(李庆)[1], Yongze Ye(叶永泽)[1], Zhiwei Wang(王秩伟)[2,3,4*], Yugui Yao(姚裕贵)[2,3], and Hai-Hu Wen(闻海虎)[1*]

[1]*National Laboratory of Solid State Microstructures and Department of Physics, Collaborative Innovation Center of Advanced Microstructures, Nanjing University, Nanjing 210093, China*
[2]*Key Laboratory of Advanced Optoelectronic Quantum Architecture and Measurement, Ministry of Education, School of Physics, Beijing Institute of Technology, Beijing 100081, China*
[3]*Micronano Center, Beijing Key Lab of Nanophotonics and Ultrafine Optoelectronic Systems, Beijing Institute of Technology, Beijing 100081, China*
[4]*Material Science Center, Yangtze Delta Region Academy of Beijing Institute of Technology, Jiaxing 314011, China*

(Received 12 September 2024; accepted manuscript online 4 November 2024)

In this study, Kagome superconductors, i.e., CsV_3Sb_5 single crystals and its Ta-doped variant, $Cs(V_{0.86}Ta_{0.14})_3Sb_5$, were studied in detail via specific heat measurements. Results revealed that the charge density wave (CDW) was suppressed and the superconducting transition temperature (T_c) considerably increased from 2.8 to 4.6 K upon Ta doping. The electronic specific heat of CsV_3Sb_5 was fitted with a model comprising an s-wave gap and a highly anisotropic extended s-wave gap, where $2\Delta/k_BT_c$ was smaller than the weak coupling limit of 3.5. $Cs(V_{0.86}Ta_{0.14})_3Sb_5$ exhibited two isotropic s-wave gaps and yielded a larger gap of $2\Delta/k_BT_c = 5.04$, indicating a significant enhancement in superconducting coupling. This evolution was attributed to the increased density of states near the Fermi level released by CDW gap suppression. These findings demonstrated that Ta doping enhanced superconducting coupling and variation of gap structure in CsV_3Sb_5.

DOI: 10.1088/0256-307X/41/12/127301

1. Introduction. AV_3Sb_5 (A = K, Rb, and Cs), a newly discovered material,[1] has garnered considerable attention owing to its unique crystal structure. This material comprises V–Sb sheets that are separated by A-ion layers. In the V–Sb sheets, the V atoms form a Kagome lattice, which is a network of corner-sharing triangles and provides the material with distinct electronic structures. Angle-resolved photoemission spectroscopy (ARPES)[2–11] and density functional theory (DFT)[2,12–14] calculations revealed that AV_3Sb_5 exhibited a multiband structure with several energy bands crossing the Fermi level. Among them, V 3d and Sb 5p orbital electrons primarily contributed to the electronic states near the Fermi surface. An electron pocket near the Γ point in the Brillouin zone originated from the p_z orbitals of Sb atoms. Near the M point, two van Hove singularities (VHSs) composed of multiple V d orbitals were observed, including d_{xy}, $d_{x^2-y^2}$, and d_{z^2}. The Dirac cone near the K point resulted from the d_{xz} and d_{yz} orbitals of V atoms. Such electronic states endow the material with several intriguing phenomena such as the charge density wave (CDW),[15–18] anomalous Hall effect (AHE),[19–21] superconductivity,[2,4,22,23] nontrivial band topology,[4,24] charge-4e and charge-6e flux quantization,[25,26] and residual Fermi arcs.[27] The competition between CDW and superconductivity is the most intriguing property, and exploring their connections and interactions is crucial for elucidating the underlying physical mechanisms of AV_3Sb_5.

The CDW and superconducting states of AV_3Sb_5 can be modulated via elemental doping. Doping can introduce positive or negative pressures that change the lattice constant and the band structure or charge carriers that affect the position of the Fermi surface. For instance, Ti or Sn doping in CsV_3Sb_5 introduces holes,[28–30] which causes double-dome superconductivity and progressively suppresses CDW. Cr or Mo doping introduces electrons[31,32] in the material; Nb and Ta are isovalent dopants[33,34] and have different effects. By comparing the superconducting gap structure and coupling strength before and after doping along with the corresponding changes in the CDW state and analyzing the differences in the Fermi surface and band structure, the mechanisms and origins of these states can be further studied.

The pairing symmetry and gap structure in CsV_3Sb_5 are debatable although these properties have been extensively studied. Some evidence supports isotropic s-wave gaps. For instance, self-field critical current ($I_{c,sf}$) measurements are consistent with the model of a single conventional s-wave gap.[35] Techniques such as muon-spin relaxation/rotation (μSR) measurements,[36,37] soft point-contact spectroscopy (SPCS),[38] specific heat measurements,[39] and tunnel diode oscillators (TDO)[39] also suggest the presence of two-gap s-wave superconductivity in CsV_3Sb_5. Gap anisotropy was also de-

*Corresponding author. Email: zhiweiwang@bit.edu.cn; hhwen@nju.edu.cn
© 2024 Chinese Physical Society and IOP Publishing Ltd

tected in CsV_3Sb_5 via experiments. Scanning tunneling microscope (STM) measurements[40–43] revealed V-shaped superconducting gaps in CsV_3Sb_5, indicating significant anisotropy, whereas ARPES measurements[44] showed large anisotropy (over 80%) in the superconducting gap on one of the Fermi pockets. Despite this discrepancy, the existence of a multigap scenario in this multiband system has been supported by most studies. At present, no direct evidence indicates the presence of nodes in the superconducting gap.

The low-energy quasiparticle excitations as well as the order parameter and electronic states near the Fermi energy can be analyzed via specific heat measurements. Herein, these measurements were conducted on CsV_3Sb_5 and $Cs(V_{0.86}Ta_{0.14})_3Sb_5$ single crystals, which indicated that doping increased T_c from 2.8 to 4.6 K. Findings also revealed the suppression of the CDW order in $Cs(V_{0.86}Ta_{0.14})_3Sb_5$, confirming its competition with the superconducting state. The low-temperature specific heat of $Cs(V_{0.86}Ta_{0.14})_3Sb_5$ increased below 1 K due to a Schottky anomaly caused by the Zeeman splitting of Ta ions. The analysis of electronic specific heat of pristine sample revealed that its gap structure could be fitted with an isotropic s-wave gap and a highly anisotropic extended s-wave gap (anisotropy parameter $\alpha = 0.8$), with $2\Delta/k_BT_c$ values of 2.98 and 2.49; these findings were consistent with the weak-coupling BCS theory. In contrast, the gap structure for in $Cs(V_{0.86}Ta_{0.14})_3Sb_5$ transforms into two isotropic s-wave gaps with $2\Delta/k_BT_c = 3.08$ and 5.04, where a larger gap corresponds to a strong-coupling superconducting pairing resulting from an increase in the density of states (DOS) at the Fermi level associated with the CDW order suppression.

2. Results. Figures 1(a) and 1(b) show the magnetization data of CsV_3Sb_5 and $Cs(V_{0.86}Ta_{0.14})_3Sb_5$ measured in zero-field-cooling (ZFC) and field-cooling (FC) modes at magnetic fields of 3 and 5 Oe, respectively. Both samples exhibited sharp superconducting transitions, indicative of their high quality. Diamagnetic transition occurred at 3.2 K for the pristine CsV_3Sb_5 and increased to 5.0 K after 14% Ta doping. The relation between T_c and Ta doping concentration in $Cs(V_{1-x}Ta_x)_3Sb_5$ was reported in a previous study,[45] which showed that T_c increased with Ta doping concentration until reaching the doping limit of 16%.

Ta doping also affected the CDW behavior in CsV_3Sb_5. Resistivity, magnetization, and specific heat measurements revealed an obvious CDW transition was observed in pristine CsV_3Sb_5 at 94 K.[2] Resistivity measurements showed that CDW gradually weakened with Ta doping and eventually suppressed when 10% Ta was doped.[45] $Cs(V_{0.86}Ta_{0.14})_3Sb_5$ was primarily studied herein. Figure 1(c) shows the specific heat data of $Cs(V_{0.86}Ta_{0.14})_3Sb_5$ from 2 to 175 K; no detectable phase transition was observed at this temperature range, which further confirmed the CDW order suppression in terms of specific heat.

The specific heat of pristine CsV_3Sb_5 and doped $Cs(V_{0.86}Ta_{0.14})_3Sb_5$ was measured from 0.4 K to 6 K. Phonons, electrons, and magnons contribute to the specific heat of a material. Electronic specific heat provides information on the gap structure and pairing symmetry of materials. By comparing the gap structures between pristine and doped samples and combining them with the Fermi surfaces and energy band structures, the effect of Ta doping on the gap structure can be elucidated. Moreover, the influence of energy bands near the Fermi surface on the superconducting energy gaps can be analyzed. Figures 2(a) and 2(b) show the C/T versus T curve that provide the specific heat data for CsV_3Sb_5 and $Cs(V_{0.86}Ta_{0.14})_3Sb_5$, respectively. The square symbols denote the data at 0 T, which exhibit evident specific heat jumps at 2.8 and 4.6 K, respectively. To suppress the superconductivity, 2 and 4 T magnetic fields were applied on these samples, as indicated with circle symbols. Superconducting signals were not observed above 0.4 K in both samples under these magnetic fields.

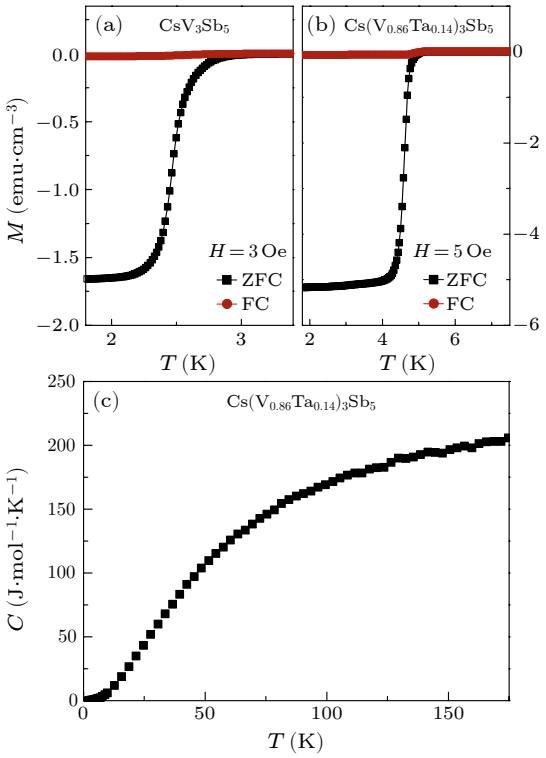

Fig. 1. Temperature dependence of magnetization for (a) CsV_3Sb_5 and (b) $Cs(V_{0.86}Ta_{0.14})_3Sb_5$ in ZFC and FC modes. (c) Temperature dependence of specific heat for $Cs(V_{0.86}Ta_{0.14})_3Sb_5$ from 2 to 175 K.

The electronic specific heat was determined by approximating the phonon component and subtracting it from the total specific heat using the Debye model. The normal-state specific heat used during analysis can be represented as follows:

$$C = \gamma_n T + \beta T^3 + \delta T^5,$$

where the first term represents the electronic contribution and the latter two terms account for the phonon part. γ_n, β, and δ are temperature-independent fitting parameters. The Sommerfeld constant γ_n describes the DOS near the

Fermi surface in the normal state; the corresponding values are shown in Table 1. The solid lines in Figs. 2(a) and 2(b) denote the fitted results of the specific heat in the normal state, which closely match the experimental results under magnetic fields. The inset in Fig. 2(b) shows the specific heat of $Cs(V_{0.86}Ta_{0.14})_3Sb_5$ under various magnetic fields. Figures 2(c) and 2(d) show the electronic specific heat curve at 0 T for CsV_3Sb_5 and the specific heat curves exhibiting low-temperature upturns for $Cs(V_{0.86}Ta_{0.14})_3Sb_5$ after subtracting the phonon component from the total specific heat, respectively. The upturn indicated that significant magnetic contributions also affected the specific heat besides the electronic contribution. The observed anomaly at low temperatures was attributed to the Schottky anomaly, which is subsequently discussed.

The open symbols in Figs. 2(b) and 2(d) show a deviating trend, which was induced by poor temperature controlling as the temperature is close to the boiling point of liquid helium (LHe).

The BCS model can be used to describe the electronic specific heat of samples as follows:

$$\gamma_e = \frac{4N(E_F)}{k_B T^3}\int_0^{+\infty}\int_0^{2\pi}\frac{e^{\xi/k_BT}}{(1+e^{\xi/k_BT})^2}\cdot(\epsilon^2+\Delta^2(\theta,T)-\frac{T}{2}\frac{d\Delta^2(T,\theta)}{dT})d\theta d\epsilon,$$

where γ_e is the electronic specific heat coefficient, $\xi = \sqrt{\epsilon^2+\Delta^2(T,\theta)}$, and $\epsilon = \frac{\hbar^2k^2}{2m} - E_F$. The gap function $\Delta(T,\theta)$ varies with different gap structures. For instance, a single s-wave gap is represented as $\Delta(T,\theta) = \Delta_0(T)$, a single d-wave gap as $\Delta(T,\theta) = \Delta_0(T)\cos 2\theta$, and a single extended s-wave as $\Delta(T,\theta) = \Delta_0(T)(1+\alpha\cos 2\theta)$, where α indicates anisotropy. If $\alpha = 1$, the gap function has accidental nodes, whereas $\alpha \approx 0$ indicates minimal anisotropy that results in an isotropic s-wave gap.

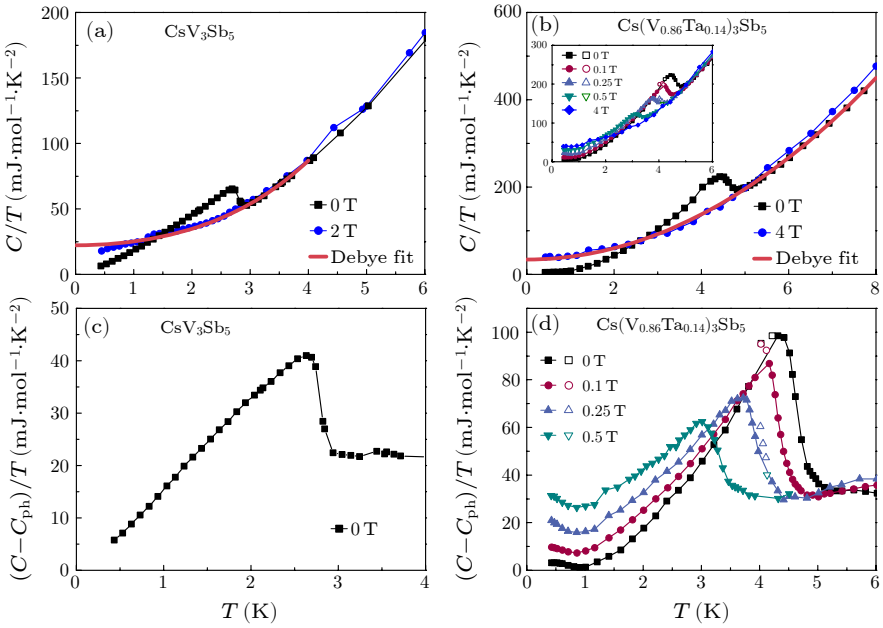

Fig. 2. Temperature dependence of specific heat plotted as C/T versus T for (a) CsV_3Sb_5 and (b) $Cs(V_{0.86}Ta_{0.14})_3Sb_5$. The solid lines represent the fitted data according to the Debye model. The inset in (b) shows the specific heat under various magnetic fields. Temperature dependence of specific heat after subtracting their phonon contributions for (c) CsV_3Sb_5 and (d) $Cs(V_{0.86}Ta_{0.14})_3Sb_5$. The open symbols in (b) and (d) denote the error points around 4 K.

Figure 3 shows the results of applying the BCS formula to CsV_3Sb_5. The specific heat was fitted using a one-gap model [Figs. 3(a) and 3(b)]. The single isotropic s-wave gap and extended s-wave gap did not fit the data, whereas the single d-wave gap fitted the data well. However, the single d-wave model exhibited several issues. The sample did not exhibit any residual zero-temperature specific heat coefficient γ_0, inconsistent with the characteristics of a d-wave superconductor. The gap nodes in a d-wave superconductor easily excites quasiparticles at low temperatures that result in a residual γ_0. ARPES and DFT calculations [2–14] revealed that the Fermi surface of CsV_3Sb_5 comprised a circular sheet formed by Sb 5p electrons as well as a triangle and hexagonal sheet formed by V 3d electrons. This multiband structure probably provided CsV_3Sb_5 with a multigap feature. The results of specific heat measurements, [39] TDO, [39] μSR, [36,37] and ARPES [44] also revealed the multigap feature of CsV_3Sb_5. Thus, a single d-wave gap model may not explain the specific heat with a complicated band structure and multiple components and a two-gap model may have to be considered. Figure 3(c) shows a model with two isotropic s-wave gaps, which roughly fitted the data with a larger gap $\Delta_1 = 0.425$ meV and a smaller gap $\Delta_2 = 0.145$ meV. The smaller gap was required for fitting data at extremely low temperatures. However, a slight discrepancy was observed

between the fitted curve and experimental data above 2 K; the fitted curve was slightly higher than the experimental data. To ensure perfect match, the fitted curve below 0.4 K must gradually decrease based on the entropy conservation principle. This indicated that a smaller gap minimum is required. Thus, a fitting model with an isotropic s-wave gap and an extended s-wave gap was developed [Fig. 3(d)], which could perfectly fit data with an isotropic s-wave gap of 0.36 meV and an extended s-wave gap of 0.30 meV with an anisotropy parameter $\alpha = 0.8$.

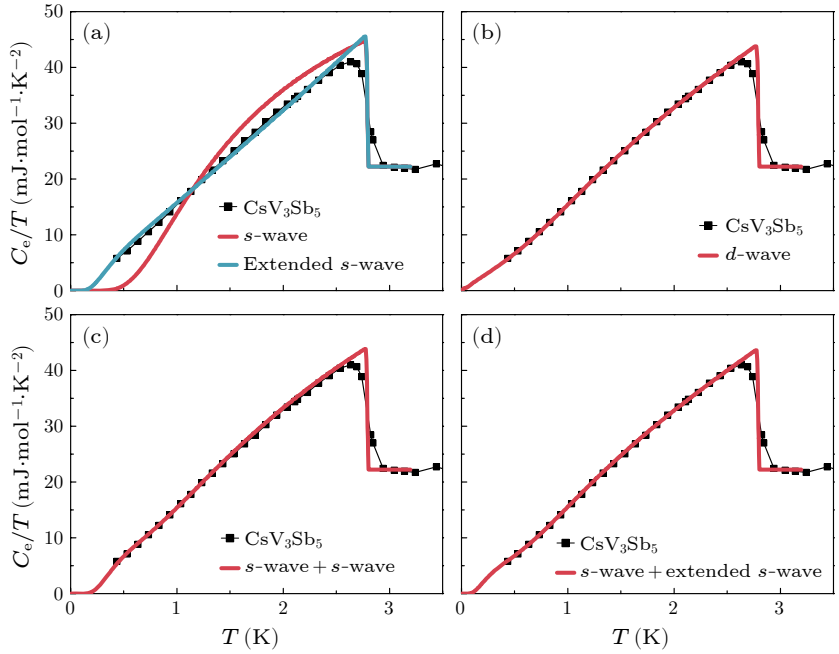

Fig. 3. Temperature dependence of electronic specific heat coefficient for CsV_3Sb_5 and the BCS fitted results with (a), (b) one-gap model and (c), (d) two-gap model.

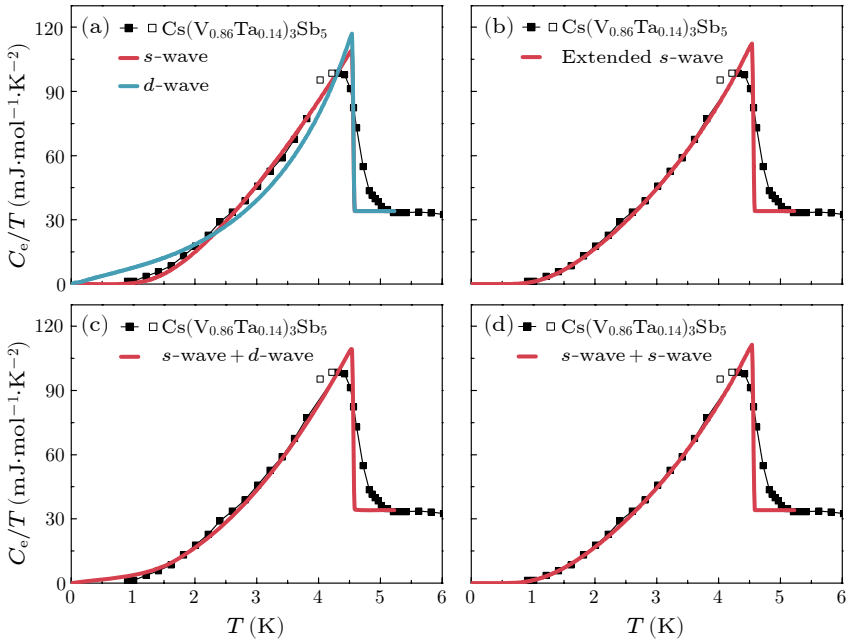

Fig. 4. Temperature dependence of electronic specific heat coefficient above 1 K for $Cs(V_{0.86}Ta_{0.14})_3Sb_5$ and the BCS fitting results with the (a), (b) one-gap model and (c), (d) two-gap model. The two open symbols are the error points.

The three fitting methods were analyzed, which indicated that the gap structure of CsV_3Sb_5 must include a very small energy gap (∼0.145 meV) or the presence of gap minima. As the two s-wave gap model was not as perfect as the other two models and the d-wave fit exhibited several issues, the gap structure in CsV_3Sb_5 was considered

to have an *s*-wave gap and a highly anisotropic extended *s*-wave gap. These findings were consistent with experimental results. For instance, a recent ARPES experiment [44] detected a superconducting gap with an anisotropy of >80%, agreeing with the results reported herein. STM measurements [40–43] further revealed V-shaped superconducting gaps, indicating significant anisotropy in the gap structure.

After subtracting the phonon contribution from the total specific heat, the data for $Cs(V_{0.86}Ta_{0.14})_3Sb_5$ revealed an upturn below 1 K [Fig. 2(d)] possibly caused by a Schottky anomaly. This anomaly complicated BCS fitting and was therefore ruled out in the fitting process. The 0 T curve in Fig. 2(d) shows that the specific heat coefficient is almost zero at 1 K, and the upturn appears below this temperature. This indicates that the specific heat below 1 K mainly resulted from the Schottky anomaly, whereas that above 1 K mainly resulted from the electronic state. Therefore, the data above 1 K were considered for BCS fitting (Fig. 4).

The BCS fitting results of $Cs(V_{0.86}Ta_{0.14})_3Sb_5$ and CsV_3Sb_5 were considerably different. A single *s*-wave and *d*-wave gap could not fit the data in one-gap models. When introducing a slight anisotropy of $\alpha = 0.3$ to the *s*-wave gap, the data can be well fitted with the curve. As CsV_3Sb_5 has multigap characteristics, a two-gap model was used for $Cs(V_{0.86}Ta_{0.14})_3Sb_5$. As shown in Fig. 4(c), the model of an *s*-wave gap and a *d*-wave gap could not fit the measurement data. Fig. 4(d) shows the fit of two isotropic *s*-wave gaps with gap values of 0.61 and 1.0 meV, which perfectly match matches the experimental curve.

In summary, a single extended *s*-wave gap with low anisotropy or a model of two isotropic *s*-wave gaps could describe the electronic specific heat of $Cs(V_{0.86}Ta_{0.14})_3Sb_5$. Compared with that of CsV_3Sb_5, the gap anisotropy of $Cs(V_{0.86}Ta_{0.14})_3Sb_5$ decreased considerably. Based on multiband feature of the system and the specific heat that confirmed the presence of two gaps, the model of two isotropic *s*-wave gaps was considered ideal for $Cs(V_{0.86}Ta_{0.14})_3Sb_5$. This finding was consistent with the H_{c1} fitting result on the same sample, which indicated the presence of two isotropic *s*-wave gaps. [46] ARPES [33] and STM [43] supported the presence of nearly isotropic gap structure in $Cs(V_{0.86}Ta_{0.14})_3Sb_5$.

Low-temperature upturns were observed in the specific heat of $Cs(V_{0.86}Ta_{0.14})_3Sb_5$. Figure 5(a) shows the specific heat data for $Cs(V_{0.86}Ta_{0.14})_3Sb_5$after subtracting the phonon contributions from 0 to 1 T. The specific heat upturned at low temperatures, indicating the contribution of electronic specific heat and magnetic field on the specific heat. A two-*s*-wave-gap model was used to determine the electronic specific heat coefficient at 0 T. Therefore, the same model was used for fitting data under different magnetic fields at temperatures above 1 K. The solid lines in Fig. 5(a) show the best fitting obtained based on the entropy conservation theory. The fitting results for specific heat data under different magnetic fields were less accurate because the low-temperature anomaly shifted to higher temperatures as the magnetic field strength increased. This phenomenon introduced additional contributions to the electronic specific heat.

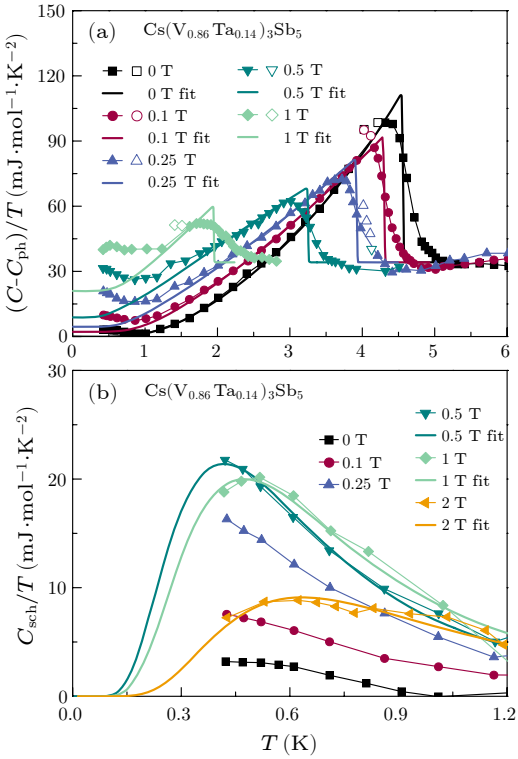

Fig. 5. (a) Temperature dependence of specific heat after subtracting phonon contributions under different magnetic fields for $Cs(V_{0.86}Ta_{0.14})_3Sb_5$. Solid lines denote the BCS fit results, and the open symbols denote the error points. (b) Magnetic specific heat coefficient of $Cs(V_{0.86}Ta_{0.14})_3Sb_5$ under different fields. Solid lines denote their Schottky fits.

Figure 5(b) shows the magnetic specific heat coefficients obtained after subtracting the electronic contributions obtained from BCS model fitting; these findings indicate a two-level Schottky anomaly caused by energy level splitting of particles in crystal or magnetic fields that produce ground and excited states. Transitions between these levels are minimal at very low temperatures. With increasing temperature, particles in the ground state have a higher probability of being excited to higher energy states and thus increase the specific heat. At considerably higher temperatures, the probabilities of these particles occupying excited states become equal and no further transitions occur; this results in a peak or bump in the Schottky specific heat. As the magnetic field increases, the Schottky peak suppresses and the weight is pushed to higher temperatures. The data in Fig. 5(b) clearly behave in that way.

The data at 0 T or at small magnetic fields do not show a peak due to Schottky anomaly although a peak is generally observed at extremely low temperatures. In this case, a peak may appear below 0.4 K. However, the peak moves to higher temperatures at 0.5, 1, and 2 T and decreases with increasing magnetic field strength; this trend is consistent with that observed for Schottky anomaly. The data obtained at 0.5, 1, and 2 T were fitted using the two-level

Schottky specific heat formula as follows:[47]

$$C_{\rm Sch}(T,H) = n\Big(\frac{g\mu_{\rm B}H}{k_{\rm B}T}\Big)^2 \frac{e^{\frac{g\mu_{\rm B}H}{k_{\rm B}T}}}{(1+e^{\frac{g\mu_{\rm B}H}{k_{\rm B}T}})^2},$$

where n is the density of magnetic particles, g is the Landé factor, H is the effective magnetic field, and $\mu_{\rm B}$ is the Bohr magneton. As indicated by the solid lines in Fig. 5(b), the data could be well-fitted using this formula. As the Schottky anomaly was observed only in $Cs(V_{0.86}Ta_{0.14})_3Sb_5$, this phenomenon can be attributed to the Zeeman splitting of Ta ions.

3. Discussion. Table 1 shows the parameters derived by analyzing the specific heat for CsV_3Sb_5 and $Cs(V_{0.86}Ta_{0.14})_3Sb_5$. Superconductivity coexisted with the CDW order in CsV_3Sb_5; its T_c was ∼2.8 K and the CDW transition occurred at 94 K. After doping with 14% Ta, T_c increased to 4.6 K and the CDW order was suppressed. This observation proved the competition between superconductivity and CDW in the doped sample.

Table 1. Several parameters of CsV_3Sb_5 and $Cs(V_{0.86}Ta_{0.14})_3Sb_5$ for comparison.

	CsV_3Sb_5	$Cs(V_{0.86}Ta_{0.14})_3Sb_5$
T_c	2.8 K	4.6 K
CDW	√	×
Gap	s-wave ($\Delta = 0.36$ meV)	s-wave ($\Delta = 1.0$ meV)
structure	+ extended s-wave ($\Delta = 0.30$ meV, $\alpha = 0.8$)	+s-wave ($\Delta = 0.61$ meV)
$2\Delta/k_{\rm B}T_c$	2.98/2.49	5.04/3.08
γ_n	22.2 mJ·mol^{-1}·K^{-2}	34.1 mJ·mol^{-1}·K^{-2}
$\Delta C/\gamma_n T_c$	0.96	2.26

Doping also changed the gap structure. BCS fittings of specific heat revealed that the gap structure in In CsV_3Sb_5 could be described using isotropic s-wave gap and extended s-wave gap models with an anisotropy of 0.8. After Ta doping, the gap structure evolved into two isotropic s-wave gaps. This finding was consistent with those derived via STM[43] and ARPES.[33,44] STM[43] revealed a V-shape superconducting gap in CsV_3Sb_5, indicating the existence of significant gap minima and quasiparticle excitations. This V-shape gap transformed into a U-shaped gap as the Ta doping concentration increased, indicating its almost isotropic nature. ARPES[33,44] also revealed that a gap with over 80% anisotropy existed on the hexagonal pocket (β pocket) at the Γ point in CsV_3Sb_5. Moreover, isotropic gaps were observed on both the circular Fermi pocket (α pocket) at the Γ point and the triangular pocket (δ pocket) at the K point. For $Cs(V_{0.86}Ta_{0.14})_3Sb_5$, the anisotropic gap on the β pocket evolved to become isotropic. By combining the BCS fitting and ARPES results for CsV_3Sb_5, the extended s-wave gap with an anisotropy of 0.8 was deemed to correspond to the gap on the β pocket; this gap resulted from the V 3d orbital and the isotropic s-wave gap possibly resulted from the α or δ pocket.

The superconducting pairing strength in CsV_3Sb_5 and $Cs(V_{0.86}Ta_{0.14})_3Sb_5$ were analyzed by calculating the value of $2\Delta/k_{\rm B}T_c$. For CsV_3Sb_5, the two gaps yielded the $2\Delta/k_{\rm B}T_c$ values of 2.98 and 2.49, which were smaller than the weak coupling limit of 3.5. For $Cs(V_{0.86}Ta_{0.14})_3Sb_5$, the $2\Delta/k_{\rm B}T_c$ values increased to 5.04 and 3.08; these values corresponded to the gaps of 1.0 and 0.61 meV. The large gap of 1.0 meV in the doped sample was caused by strong coupling. The value of $\Delta C/\gamma_n T_c$ was also calculated to determine the pairing strength. CsV_3Sb_5 exhibited a $\Delta C/\gamma_n T_c$ value of 0.96, consistent with the weak coupling theory (smaller than 1.43). $Cs(V_{0.86}Ta_{0.14})_3Sb_5$ exhibited a $\Delta C/\gamma_n T_c$ value of 2.26, indicating strong pairing. The evolution of these parameters demonstrated that Ta doping considerably enhanced the superconducting pairing strength and the Sommerfeld constant γ_n from 22.2 mJ·mol^{-1}·K^{-2} in CsV_3Sb_5 to 34.1 mJ·mol^{-1}·K^{-2} in $Cs(V_{0.86}Ta_{0.14})_3Sb_5$ with doping. As γ_n was directly related to the DOS near the Fermi level, this increase in γ_n reflected a corresponding increase in the DOS at the Fermi level. A higher DOS indicated that more electronic states participated in the superconducting pairing, which enhanced the coupling observed in the doped sample.

The stronger superconducting pairing was closely linked to the interplay between CDW and superconductivity. The DOS near the Fermi level reduced by the opening of the CDW gap In CsV_3Sb_5, which suppressed the electronic states that participated in pairing. However, Ta doping weakened the CDW state and formed more DOS near the Fermi surface, which enhanced the superconductivity. These findings confirmed that doping enhanced the DOS and superconducting pairing strength in $Cs(V_{0.86}Ta_{0.14})_3Sb_5$. Moreover, enhanced superconducting coupling caused changes in the electronic structure related to CDW suppression.

CDW formation in CsV_3Sb_5 was primarily associated with Fermi surface nesting between VHSs[9,12,48] or electron–phonon coupling.[10,49,50] During Fermi surface nesting, the hexagonal Fermi surface of the Kagome lattice became unstable as the band filling approached the VHS and resulted in a CDW state that opened the gap at the Fermi surface. It also considerably reduced the DOS near the Fermi level. This condition changed after Ta doping. For instance, ARPES revealed that Ti dopants in $Cs(V_{1-x}Ti_x)_3Sb_5$ induced holes and pushed the VHS above the Fermi level, thereby disrupting nesting and suppressing the CDW state. Consequently, the gapped DOS was released and γ_n increased.[48] However, Ta doping behaves differently. Ta was isovalent with V, but it lost electrons easily. Thus, Ta doping induced moderate number of electrons to the Kagome lattice, which possibly did not push the VHS above the Fermi level.

The ARPES of $CsV_{3-x}Ta_xSb_5$ (x about 0.4) revealed that the VHS did not move above the Fermi surface but perfectly aligned with the Fermi level. This created a flat dispersion at the Fermi surface, thereby considerably increasing the DOS that participated in superconducting pairing[11] and enhanced it. If the VHS were precisely on the Fermi surface, Fermi surface nesting would sustain. However, CDW was suppressed, which contradicted the finding that CDW was induced by the nesting of the momentum zones of VHS. This also indicated that other mechanisms, such as electron–phonon interactions or electronic correlations, possibly played a role in the formation of CDW in $CsV_{3-x}Ta_xSb_5$.

4. Conclusion. In summary, specific heat measurements of CsV_3Sb_5 single crystals and $Cs(V_{0.86}Ta_{0.14})_3Sb_5$ were performed herein. Results revealed that Ta doping increased T_c and suppressed the CDW order. The low-temperature specific heat in $Cs(V_{0.86}Ta_{0.14})_3Sb_5$ exhibited a Schottky anomaly that possibly resulted from the Zeeman splitting of Ta ions. The BCS fittings of the electronic specific heat of both samples revealed changes in their gap structure from an isotropic and anisotropic s-wave gap (with anisotropy of 0.8) to two isotropic s-wave gaps. Moreover, $2\Delta/k_BT_c$ values showed an enhanced superconducting coupling with Ta doping. The analysis of the band structure revealed that this enhanced superconductivity was caused by an increase in the DOS near the Fermi surface influenced by the CDW gap.

Materials and Methods. CsV_3Sb_5 and $Cs(V_{0.86}Ta_{0.14})_3Sb_5$ single crystals were grown using the self-flux method.[1,2,33] Magnetization was measured using a superconducting quantum interference device (SQUID-VSM, Quantum Design), and the specific heat was measured using a physical property measurement system (Quantum Design) via the thermal relaxation method.

Acknowledgements. This work was supported by the National Key R&D Program of China (Grant Nos. 2022YFA1403201, 2022YFA1403400, and 2020YFA0308800), the National Natural Science Foundation of China (Grant Nos. 11927809, 12061131001, 11974171, 92065109, and 12204231), the Fundamental Research Funds for the Central Universities (Grant No. 020414380208). Z.W. thanks the Analysis & Testing Center at BIT for assistance in facility support.

References

[1] Ortiz B R, Gomes L C, Morey J R, Winiarski M, Bordelon M, Mangum J S, Oswald I W H, Rodriguez-Rivera J A, Neilson J R, Wilson S D, Ertekin E, McQueen T M, and Toberer E S 2019 *Phys. Rev. Mater.* **3** 094407
[2] Ortiz B R, Teicher S M L, Hu Y, Zuo J L, Sarte P M, Schueller E C, Abeykoon A M M, Krogstad M J, Rosenkranz S, Osborn R, Seshadri R, Balents L, He J, and Wilson S D 2020 *Phys. Rev. Lett.* **125** 247002
[3] Cho S, Ma H, Xia W, Yang Y, Liu Z, Huang Z, Jiang Z, Lu X, Liu J, Liu Z, Li J, Wang J, Liu Y, Jia J, Guo Y, Liu J, and Shen D 2021 *Phys. Rev. Lett.* **127** 236401
[4] Liu Z, Zhao N, Yin Q, Gong C, Tu Z, Li M, Song W, Liu Z, Shen D, Huang Y, Liu K, Lei H, and Wang S 2021 *Phys. Rev. X* **11** 041010
[5] Nakayama K, Li Y, Kato T, Liu M, Wang Z, Takahashi T, Yao Y, and Sato T 2021 *Phys. Rev. B* **104** L161112
[6] Hu Y, Wu X, Ortiz B R, Han X, Plumb N C, Wilson S D, Schnyder A P, and Shi M 2022 *Phys. Rev. B* **106** L241106
[7] Hu Y, Wu X, Ortiz B R, Ju S, Han X, Ma J, Plumb N C, Radovic M, Thomale R, Wilson S D, Schnyder A P, and Shi M 2022 *Nat. Commun.* **13** 2220
[8] Kang M, Fang S, Kim J K, Ortiz B R, Ryu S H, Kim J, Yoo J, Sangiovanni G, Sante D D, Park B G, Jozwiak C, Bostwick A, Rotenberg E, Kaxiras E, Wilson S D, Park J H, and Comin R 2022 *Nat. Phys.* **18** 301
[9] Lou R, Fedorov A, Yin Q, Kuibarov A, Tu Z, Gong C, Schwier E F, Büchner B, Lei H, and Borisenko S 2022 *Phys. Rev. Lett.* **128** 036402
[10] Luo H, Gao Q, Liu H, Gu Y, Wu D, Yi C, Jia J, Wu S, Luo X, Xu Y, Zhao L, Wang Q, Mao H, Liu G, Zhu Z, Shi Y, Jiang K, Hu J, Xu Z, and Zhou X J 2022 *Nat. Commun.* **13** 273
[11] Luo Y, Han Y, Liu J, Chen H, Huang Z, Huai L, Li H, Wang B, Shen J, Ding S, Li Z, Peng S, Wei Z, Miao Y, Sun X, Ou Z, Xiang Z, Hashimoto M, Lu D, Yao Y, Yang H, Chen X, Gao H J, Qiao Z, Wang Z, and He J 2023 *Nat. Commun.* **14** 3819
[12] Tan H, Liu Y, Wang Z, and Yan B 2021 *Phys. Rev. Lett.* **127** 046401
[13] LaBollita H and Botana A S 2021 *Phys. Rev. B* **104** 205129
[14] Ortiz B R, Teicher S M L, Kautzsch L, Sarte P M, Ratcliff N, Harter J, Ruff J P C, Seshadri R, and Wilson S D 2021 *Phys. Rev. X* **11** 041030
[15] Mielke C, Das D, Yin J X, Liu H, Gupta R, Jiang Y X, Medarde M, Wu X, Lei H, and Chang J 2022 *Nature* **602** 245
[16] Xu Y, Ni Z, Liu Y, Ortiz B R, Deng Q, Wilson S D, Yan B, Balents L, and Wu L 2022 *Nat. Phys.* **18** 1470
[17] Li H, Zhang T T, Yilmaz T, Pai Y Y, Marvinney C E, Said A, Yin Q W, Gong C S, Tu Z J, Vescovo E, Nelson C S, Moore R G, Murakami S, Lei H C, Lee H N, Lawrie B J, and Miao H 2021 *Phys. Rev. X* **11** 031050
[18] Jiang Y X, Yin J X, Denner M M, Shumiya N, Ortiz B R, Xu G, Guguchia Z, He J, Hossain M S, Liu X, Ruff J, Kautzsch L, Zhang S S, Chang G, Belopolski I, Zhang Q, Cochran T A, Multer D, Litskevich M, Cheng Z J, Yang X P, Wang Z, Thomale R, Neupert T, Wilson S D, and Hasan M Z 2021 *Nat. Mater.* **20** 1353
[19] Yang S Y, Wang Y, Ortiz B R, Liu D, Gayles J, Derunova E, Gonzalez-Hernandez R, Šmejkal L, Chen Y, Parkin S S P, Wilson S D, Toberer E S, McQueen T, and Ali M N 2020 *Sci. Adv.* **6** eabb6003
[20] Yu F H, Wu T, Wang Z Y, Lei B, Zhuo W Z, Ying J J, and Chen X H 2021 *Phys. Rev. B* **104** L041103
[21] Zhao H, Li H, Ortiz B R, Teicher S M, Park T, Ye M, Wang Z, Balents L, Wilson S D, and Zeljkovic I 2021 *Nature* **599** 216
[22] Ortiz B R, Sarte P M, Kenney E M, Graf M J, Teicher S M, Seshadri R, and Wilson S D 2021 *Phys. Rev. Mater.* **5** 034801
[23] Yin Q, Tu Z, Gong C, Fu Y, Yan S, and Lei H 2021 *Chin. Phys. Lett.* **38** 037403
[24] Shrestha K, Chapai R, Pokharel B K, Miertschin D, Nguyen T, Zhou X, Chung D Y, Kanatzidis M G, Mitchell J F, Welp U, Popović D, Graf D E, Lorenz B, and Kwok W K 2022 *Phys. Rev. B* **105** 024508
[25] Zhou S and Wang Z 2022 *Nat. Commun.* **13** 7288
[26] Ge J, Wang P, Xing Y, Yin Q, Wang A, Shen J, Lei H, Wang Z, and Wang J 2024 *Phys. Rev. X* **14** 021025
[27] Deng H, Qin H, Liu G, Yang T, Fu R, Zhang Z, Wu X, Wang Z, Shi Y, Liu J, Liu H, Yan X Y, Song W, Xu X, Zhao Y, Yi M, Xu G, Hohmann H, Holbæk S C, Dürrnagel M, Zhou S, Chang G, Yao Y, Wang Q, Guguchia Z, Neupert T, Thomale R, Fischer M H, and Yin J X 2024 *Nature* **632** 775
[28] Sur Y, Kim K T, Kim S, and Kim K H 2023 *Nat. Commun.* **14** 3899

[29] Yang H, Huang Z, Zhang Y, Zhao Z, Shi J, Luo H, Zhao L, Qian G, Tan H, Hu B, Zhu K, Lu Z, Zhang H, Sun J, Cheng J, Shen C, Lin X, Yan B, Zhou X, Wang Z, Pennycook S J, Chen H, Dong X, Zhou W, and Gao H J 2022 *Sci. Bull.* **67** 2176

[30] Oey Y M, Ortiz B R, Kaboudvand F, Frassineti J, Garcia E, Cong R, Sanna S, Mitrović V F, Seshadri R, and Wilson S D 2022 *Phys. Rev. Mater.* **6** L041801

[31] Ding G, Wo H, Gu Y, Gu Y, and Zhao J 2022 *Phys. Rev. B* **106** 235151

[32] Liu M, Han T, Hu X, Tu Y, Zhang Z, Long M, Hou X, Mu Q, and Shan L 2022 *Phys. Rev. B* **106** L140501

[33] Zhong Y, Liu J, Wu X, Guguchia Z, Yin J X, Mine A, Li Y, Najafzadeh S, Das D, Mielke III C, Khasanov R, Luetkens H, Suzuki T, Liu K, Han X, Kondo T, Hu J, Shin S, Wang Z, Shi X, Yao Y, and Okazaki K 2023 *Nature* **617** 488

[34] Xiao Q, Li Q, Liu J, Li Y, Xia W, Zheng X, Guo Y, Wang Z, and Peng Y 2023 *Phys. Rev. Mater.* **7** 074801

[35] Zhang W, Liu X, Wang L, Tsang C W, Wang Z, Lam S T, Wang W, Xie J, Zhou X, Zhao Y, Wang S, Tallon J, Lai K T, and Goh S K 2023 *Nano. Lett.* **23** 872

[36] Shan Z, Biswas P K, Ghosh S K, Tula T, Hillier A D, Adroja D, Cottrell S, Cao G H, Liu Y, Xu X, Song Y, Yuan H, and Smidman M 2022 *Phys. Rev. Res.* **4** 033145

[37] Gupta R, Das D, Mielke III C H, Guguchia Z, Shiroka T, Baines C, Bartkowiak M, Luetkens H, Khasanov R, Yin Q, Tu Z, Gong C, and Lei H 2022 *npj Quantum Mater.* **7** 49

[38] Yin L, Zhang D, Chen C, Ye G, Yu F, Ortiz B R, Luo S, Duan W, Su H, Ying J, Wilson S D, Chen X, Yuan H, Song Y, and Lu X 2021 *Phys. Rev. B* **104** 174507

[39] Duan W, Nie Z, Luo S, Yu F, Ortiz B R, Yin L, Su H, Du F, Wang A, Chen Y, Lu X, Ying J, Wilson S D, Chen X, Song Y, and Yuan H 2021 *Sci. China Phys. Mech. Astron.* **64** 107462

[40] Chen H, Yang H, Hu B, Zhao Z, Yuan J, Xing Y, Qian G, Huang Z, Li G, Ye Y, Ma S, Ni S, Zhang H, Yin Q, Gong C, Tu Z, Lei H, Tan H, Zhou S, Shen C, Dong X, Yan B, Wang Z, and Gao H J 2021 *Nature* **599** 222

[41] Liang Z, Hou X, Zhang F, Ma W, Wu P, Zhang Z, Yu F, Ying J J, Jiang K, Shan L, Wang Z, and Chen X H 2021 *Phys. Rev. X* **11** 031026

[42] Xu H S, Yan Y J, Yin R, Xia W, Fang S, Chen Z, Li Y, Yang W, Guo Y, and Feng D L 2021 *Phys. Rev. Lett.* **127** 187004

[43] Hu B, Chen H, Ye Y, Huang Z, Han X, Zhao Z, Xiao H, Lin X, Yang H, Wang Z, and Gao H J 2024 *Nat. Commun.* **15** 6109

[44] Mine A, Zhong Y, Liu J, Suzuki T, Najafzadeh S, Uchiyama T, Yin J X, Wu X, Shi X, Wang Z, Yao Y, and Okazaki1 K 2024 arXiv:2404.18472 [cond-mat.supr-con]

[45] Liu J, Li Q, Li Y, Fan X, Li J, Zhu P, Deng H, Yin J X, Yang H, Li J, Wen H H, and Wang Z 2024 *Scientific Reports* **14** 9580

[46] Li J, Xie W, Liu J, Li Q, Li X, Yang H, Wang Z, Yao Y, and Wen H H 2022 *Phys. Rev. B* **106** 214529

[47] Gao H, Wang Y, Shan L, Yao X, and Wen H H 2005 *Physica C: Superconductivity* **432** 293

[48] Liu Y, Wang Y, Cai Y, Hao Z, Ma X M, Wang L, Liu C, Chen J, Zhou L, Wang J, Wang S, He H, Liu Y, Cui S, Huang B, Wang J, Chen C, and Mei J W 2023 *Phys. Rev. Mater.* **7** 064801

[49] Xie Y, Li Y, Bourges P, Ivanov A, Ye Z, Yin J X, Hasan M Z, Luo A, Yao Y, Wang Z, Xu G, and Dai P 2022 *Phys. Rev. B* **105** L140501

[50] Ye Z, Luo A, Yin J X, Hasan M Z, and Xu G 2022 *Phys. Rev. B* **105** 245121